Joint Optimization of Sensing and Communications in Vehicular Networks: A Graph Neural Network-based Approach

*Xuefei Li, †Mingzhe Chen, *Zhilong Zhang, *Danpu Liu, ‡Yuchen Liu, and §Shiwen Mao
*Beijing Laboratory of Advanced Information Network, Beijing University of Posts and Telecommunications, Beijing, China 100876, Emails: 2013213202@bupt.edu.cn, zhilong.zhang@outlook.com, dpliu@bupt.edu.cn.
†Department of Electrical and Computer Engineering and Institute for Data Science and Computing, University of Miami, Coral Gables, FL, 33146 USA, Email: mingzhe.chen@miami.edu.
‡ Department of Computer Science, North Carolina State University, Raleigh, NC 27695 USA, Email: yuchen.liu@ncsu.edu.
§Department of Electrical and Computer Engineering, Auburn University, Auburn, AL 36849 USA, Email: smao@ieee.org.

***Abstract*—In this paper, the problem of joint sensing and communications is studied over terahertz (THz) vehicular networks. In the studied model, a set of service provider vehicles provide either communication service or sensing service to communication target vehicles or sensing target vehicles, respectively. Therefore, it is necessary to determine the service mode (i.e., providing sensing or communication service) for each service provider vehicle and the subset of target vehicles that each service provider vehicle will serve. The problem is formulated as an optimization problem aiming to maximize the sum of the data rates of all communication target vehicles while satisfying the sensing service requirements of all sensing target vehicles by determining the service mode and the user association for each service provider vehicle. To solve this problem, a graph neural network (GNN) based algorithm with a heterogeneous graph representation is proposed. The proposed algorithm enables the central controller to extract each vehicle's graph information related to its location, connection, and communication interference. Using the extracted graph information, the joint service mode selection and user association strategy will be determined. Simulation results show that the proposed GNN-based scheme can achieve 94% of the sum rate produced by the optimal solution, and yield up to 3.95% and 36.16% improvements in sum rate, respectively, compared to a homogeneous GNN-based algorithm and the conventional optimization algorithm without using GNNs.**

I. Introduction

Integration of wireless signal communication and sensing functionalities on smart vehicles has been regarded as a promising paradigm to improve the safety and efficiency of vehicular networks. The joint design of sensing and communication functionalities can mutually enhance each other by leveraging the unified hardware, spectrum resource, and protocol design [1]. However, the scarce bandwidth of sub-6 GHz bands limits the ability of wireless networks to satisfy the stringent quality-of-service (QoS) requirements of emerging vehicular applications in terms of delivering high data rate and high-resolution sensing [2]. A promising solution is to use the high frequency terahertz (THz) band for abundant bandwidth. However, using THz for joint sensing and communication in vehicular networks faces several challenges, such as severe path loss and attenuation, extremely directional nature of vehicular links, and stringent service assurance requirements.

This work is supported in part by the National Natural Science Foundation of China under Grant No.61971069 and 62271065, the Beijing Natural Science Foundation under Grant No.L202003, the Shanghai Science and Technology Commission Research Project No.20511106700, and the Open Research Project of the State Key Laboratory of Media Convergence and Communication, Communication University of China (No. SKLMCC2021KF009).

Recently, several works, such as in [3]–[6], have studied the problem of resource management for joint communication and sensing systems. However, the proposed methods in [3]–[5] might introduce mutual interference between communication and sensing systems due to inconsistent operating modes of different vehicles. To address this challenge, in [6], the authors analyzed the interference between communication and sensing services so as to optimize the time slot allocation for providing communication and sensing services to each vehicle. However, the works in [3]–[6] did not consider the use of THz bands to provide high-quality communication and high-resolution sensing services. Using THz bands can improve data transmission rate and sensing resolution. However, the THz bands have higher path loss and attenuation. Thus, it is necessary to design novel sensing and communications for vehicular networks that can overcome such limitations. The authors in [7]–[10] studied the use of THz bands for providing communication service in vehicle networks. However, none of the existing works [7]–[10] considered the use of THz bands to provide sensing service.

The main contribution of this work is to design a novel framework that enables service provider vehicles to provide joint communication and sensing services to target vehicles using THz bands. In particular, we consider a system model that consists of a set of service provider vehicles that provide either communication service or sensing service to communication target vehicles or sensing target vehicles, respectively. A central controller determines the service mode (i.e., providing sensing or communication service) for each service provider vehicle and the subset of target vehicles that each service provider vehicle will serve. We formulate an optimization problem aiming to maximize the sum of the data rates of all communication target vehicles while satisfying the sensing service requirements of sensing target vehicles by jointly determining the service mode (communication or sensing) and the user association for each service provider vehicle. To solve this problem, a GNN-based algorithm with a heterogeneous graph representation is proposed. The proposed algorithm enables the central controller to extract each vehicle's graph information that represents the information related to vehicle location, vehicle connection, and vehicle communication interference. Using the extracted graph information, the joint service mode selection and user association strategy will be determined. Simulation results show that the proposed GNN-based scheme can improve the sum rate by up to 3.95% and 36.16%, respectively, compared to

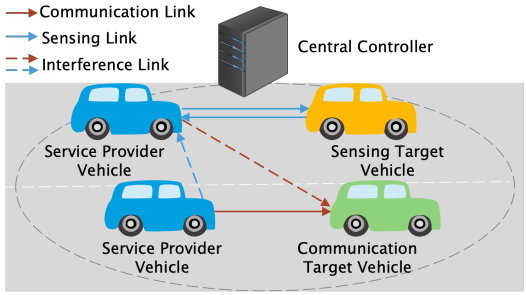

Fig. 1: Illustration of the communication and sensing links.

a homogeneous GNN-based algorithm and the conventional optimization algorithm without using GNNs.

II. System Model and Problem Formulation

A. Network Model

We consider a vehicular network in which a set of vehicles moving in a region, as shown in Fig. 1. The vehicles are divided into three categories: service provider vehicles $\mathcal{K}$, communication target vehicles $\mathcal{M}$, and sensing target vehicles $\mathcal{N}$. Each service provider vehicle is equipped with both communication and sensing devices. Therefore, each service provider vehicle can operate in either the communication mode or the sensing mode. Operating in the communication mode, a service provider vehicle can communicate with the target vehicles through vehicle-to-vehicle (V2V) links. In contrast, a service provider vehicle that operates in the sensing mode can sense the location, speed and direction of the target vehicles for further analysis (e.g. generate High-definition map (HD Map)). In our model, the locations of the vehicles and the number of vehicles vary over time with unknown distributions. We assume that all service provider vehicles use the same THz bands to provide communication or sensing services.

1) THz Propagation and Antenna Model: We assume that directional three-dimensional (3D) beams are utilized at the vehicles to compensate for the severe path loss in the THz bands. The antenna gains of the main lobe and the side lobes of the beam from vehicle k to vehicle m is expressed as [10]

$$G_{km}^{\mathrm{M}} = \frac{4\pi}{(\varepsilon+1)\Omega_{\theta_k,\varphi_k}}, \tag{1}$$

$$G_{km}^{\mathrm{S}} = \frac{4\pi\varepsilon}{(\varepsilon+1)\left(4\pi-\Omega_{\theta_k,\varphi_k}\right)}, \tag{2}$$

where $\Omega_{\theta_k,\varphi_k} = 4\arcsin\left(\tan\left(\frac{\theta_k}{2}\right)\tan\left(\frac{\varphi_k}{2}\right)\right)$ with θ_k and φ_k being the horizontal and vertical beamwidths of the antenna for vehicle k, and ε is the ratio of the power concentrated along the side lobes to the power concentrated along the main lobe.

The signal propagation at the THz band is determined by spreading loss and molecular absorption loss. The absorption loss [8] is defined as $L_{km}^{\mathrm{A}} = \frac{1}{\tau(d_{km})}$, with d_{km} being the distance between vehicle k and vehicle m. $\tau(d_{km}) \approx e^{-\phi(f)d_{km}}$ is the transmittance of the medium following the Beer-Lambert law, with $\phi(f)$ being the overall absorption coefficient of the medium, and f is the operating frequency.

Assuming free space propagation, the spreading loss is given by $L_{km}^{\mathrm{F}} = \frac{(4\pi f d_{km})^2}{c^2}$, where c is the speed of light.

Therefore, the received power at vehicle m from vehicle k is $S_{km} = \frac{P_k G_{km}^{\mathrm{T}} G_{mk}^{\mathrm{R}}}{L_{km}^{\mathrm{A}} L_{km}^{\mathrm{F}}}$, where P_k is the transmit power of vehicle k. G_{km}^{T} and G_{mk}^{R} are the effective antenna gains at vehicle k and vehicle m, respectively, corresponding to the link between vehicle k and vehicle m with $\mathrm{T} \in \{\mathrm{M},\mathrm{S}\}$ and $\mathrm{R} \in \{\mathrm{M},\mathrm{S}\}$, where M is for the main lobe and S is for the side lobes.

2) Communication Mode: The interference to the communication link between vehicle k and vehicle m is

$$\begin{aligned} I_{km}^{\mathrm{C}}(\boldsymbol{\alpha},\boldsymbol{\beta}) = &\sum_{i\in\mathcal{K}\setminus\{k\}}\sum_{m'\in\mathcal{M}} \frac{\alpha_{im'} P_i G_{im}^{\mathrm{T}} G_{mi}^{\mathrm{R}}}{L_{im}^{\mathrm{A}} L_{im}^{\mathrm{F}}}, \\ &+ \sum_{i\in\mathcal{K}\setminus\{k\}}\sum_{n'\in\mathcal{N}} \frac{\beta_{in'} P_i G_{im}^{\mathrm{T}} G_{mi}^{\mathrm{R}}}{L_{im}^{\mathrm{A}} L_{im}^{\mathrm{F}}}, \end{aligned} \tag{3}$$

where $\boldsymbol{\alpha} = [\boldsymbol{\alpha}_1, \cdots, \boldsymbol{\alpha}_M]$ with $\boldsymbol{\alpha}_m = [\alpha_{1m}, \cdots, \alpha_{Km}]$, and $\boldsymbol{\beta} = [\boldsymbol{\beta}_1, \cdots, \boldsymbol{\beta}_N]$ with $\boldsymbol{\beta}_n = [\beta_{1n}, \cdots, \beta_{Kn}]$. Here, $\boldsymbol{\alpha}$ and $\boldsymbol{\beta}$ are the mode selection and user association indicator matrices. $\alpha_{im} = 1$ represents that vehicle i is selected to serve vehicle m in the communication mode; otherwise, $\alpha_{im} = 0$. Similarly, $\beta_{in} = 1$ represents that vehicle i is selected to detect vehicle n in the sensing mode; otherwise, $\beta_{in} = 0$. In (6), the first term represents the interference from other vehicles that operate in the communication mode, while the second term is the interference from other vehicles that operate in the sensing mode.

The signal-to-interference-plus-noise ratio (SINR) between vehicle k and vehicle m is

$$\gamma_{km}^{\mathrm{C}}(\boldsymbol{\alpha},\boldsymbol{\beta}) = \frac{\alpha_{km} S_{km}}{I_{km}^{\mathrm{C}}(\boldsymbol{\alpha},\boldsymbol{\beta}) + N_{km}}, \tag{4}$$

where $N_{km} = N_0 + \sum_{i\in\mathcal{K}\setminus\{k\}} P_i G_{im}^{\mathrm{T}} G_{mi}^{\mathrm{R}} (1-\tau(d_{im}))/L_{im}^{\mathrm{F}}$ with N_0 being the Johnson-Nyquist noise power. N_{km} is caused by thermal agitation of electrons and molecular absorption.

Therefore, the data rate of vehicle k transmitting data to vehicle m is

$$R_{km}^{\mathrm{C}}(\boldsymbol{\alpha},\boldsymbol{\beta}) = B\log_2\left(1+\gamma_{km}^{\mathrm{C}}(\boldsymbol{\alpha},\boldsymbol{\beta})\right), \tag{5}$$

where B denotes the spectrum bandwidth.

3) Sensing Mode: The interference to vehicle k operating in the sensing mode can be expressed as

$$\begin{aligned} I_{kn}^{\mathrm{S}}(\boldsymbol{\alpha},\boldsymbol{\beta}) = &\sum_{i\in\mathcal{K}\setminus\{k\}}\sum_{m'\in\mathcal{M}} \frac{\alpha_{im'} P_i G_{ik}^{\mathrm{T}} G_{ki}^{\mathrm{R}}}{L_{ik}^{\mathrm{A}} L_{ik}^{\mathrm{F}}} \\ &+ \sum_{i\in\mathcal{K}\setminus\{k\}}\sum_{n'\in\mathcal{N}} \frac{\beta_{in'} P_i G_{ik}^{\mathrm{T}} G_{ki}^{\mathrm{R}}}{L_{ik}^{\mathrm{A}} L_{ik}^{\mathrm{F}}} \\ &+ \sum_{i\in\mathcal{K}\setminus\{k\}}\sum_{n'\in\mathcal{N}} \frac{\beta_{in'} P_i G_{in}^{\mathrm{T}} G_{nk}^{\mathrm{R}} \sigma_{i,n} c^2}{(4\pi)^3 f^2 d_{in}^2 d_{kn}^2 L_{in}^{\mathrm{A}} L_{kn}^{\mathrm{A}}}, \end{aligned} \tag{6}$$

where $\sigma_{i,n}$ is the target's radar cross section (RCS) between vehicle i and vehicle n. In (6), the first term represents the interference from other vehicles that operate in the communication

mode. The second term represents the interference propagating in the direct path $i \to k$ from other vehicles that operate in the sensing mode. The third term represents the interference propagating in the scattering path $i \to n \to k$ from other vehicles that operate in the sensing mode.

From (3) and (6), we can see that a vehicle that operates in the sensing mode is interfered by other vehicles that operate in the sensing mode from scattering paths, which will not interfere the vehicles that operate in communication mode. This is because the impacts of scattered sensing signals on a communication link is much weaker than that on the sensing link [6].

Given (6), the SINR of vehicle k that operates in the sensing mode when sensing vehicle n can be expressed as

$$\gamma_{kn}^{\mathrm{S}}(\boldsymbol{\alpha},\boldsymbol{\beta}) = \frac{\beta_{kn} P_k G_{kn}^{\mathrm{T}} G_{nk}^{\mathrm{R}} (L_{kn}^{\mathrm{S}})^{-1} (L_{kn}^{\mathrm{A}})^{-1}}{I_{kn}^{\mathrm{S}}(\boldsymbol{\alpha},\boldsymbol{\beta}) + N_{kn}}, \tag{7}$$

where $L_{kn}^{\mathrm{S}} = \frac{(4\pi)^3 f^2 d_{kn}^4}{\sigma_{k,n} c^2}$ is the spreading loss of the path $k \to n \to k$.

B. Problem Formulation

To maximize the data rates of all communication target vehicles while satisfying the sensing service requirement, an optimization problem is formulated as:

$$\max_{\boldsymbol{\alpha},\boldsymbol{\beta}} \sum_{k\in\mathcal{K}} \sum_{m\in\mathcal{M}} R_{km}^{\mathrm{C}}(\boldsymbol{\alpha},\boldsymbol{\beta}) \tag{8}$$

$$\text{s.t.} \sum_{k\in\mathcal{K}} \alpha_{km} = 1, \alpha_{km} \in \{0,1\}, \forall m \in \mathcal{M}, \tag{8a}$$

$$\sum_{k\in\mathcal{K}} \beta_{kn} = 1, \beta_{kn} \in \{0,1\}, \forall n \in \mathcal{N}, \tag{8b}$$

$$\sum_{m\in\mathcal{M}} \alpha_{km} \geq 0, \sum_{n\in\mathcal{N}} \beta_{kn} \geq 0, \forall k \in \mathcal{K}, \tag{8c}$$

$$\alpha_{km}\beta_{kn} = 0, \forall k \in \mathcal{K}, \forall m \in \mathcal{M}, \forall n \in \mathcal{N}, \tag{8d}$$

$$\gamma_{kn}^{\mathrm{S}}(\boldsymbol{\alpha},\boldsymbol{\beta}) \geq \gamma_{\min}, \forall k \in \mathcal{K}, \forall n \in \mathcal{N}, \tag{8e}$$

where $\gamma_{\min}$ is the minimum SINR requirement of the sensing service. In (8), constraint (8a) ensures that a communication target vehicle can only be served by one service provider vehicle. Constraint (8b) ensures that a sensing target vehicle can only be detected by one service provider vehicle. Constraint (8c) indicates that a service provider vehicle can service multiple sensing or communication target vehicles simultaneously. Constraint (8d) indicates that a service provider vehicle can operate in either the communication mode or the sensing mode. Constraint (8e) is the minimum SINR requirement of a sensing service.

Problem (8) is hard to solve due to the following reasons. First, the objective function is non-convex and hence the complexity of using traditional optimization algorithms is extremely high. Meanwhile, traditional optimization methods do not consider the dynamic vehicle topology such as the arrival of new vehicles. Therefore, when the vehicle topology changes, the central controller must execute the optimization algorithm again to optimize mode selection and user association schemes. Machine learning (ML) has been developed to learn the relationship between neighboring nodes rather than obtaining a separate feature vector for each vehicle [11]. To solve this problem, we propose to use graph neural networks to learn a function to generate the feature vector for each vehicle. It can obtain the feature vector of the new vehicle quickly without retraining. Then the new mode selection and user association strategy can be determined based on the extracted feature vector.

III. Mode Selection and User Association based on Graph Neural Network

In this section, we introduce a heterogeneous graph neural network-based algorithm to solve problem (8). First, we transform the joint mode selection and user association problem (8) into a classification problem, where service provider vehicles and target vehicles are considered as samples and classes, respectively. Since each service provider vehicle can simultaneously provide service for multiple target vehicles, the corresponding problem naturally becomes a multi-label classification problem, where each sample belongs to a set of classes. We study the use of a heterogeneous GNN-based algorithm to solve this classification problem. Next, we introduce the use of a heterogeneous graph to represent our considered system model, and then introduce the components of our designed algorithm. We will also explain the training method for the designed algorithm.

A. Graph Representation for Vehicular Networks

We first introduce the use of a heterogeneous graph to represent the considered network as a graphical model. A heterogeneous graph $\mathcal{G} = (\mathcal{V}, \mathcal{E}, \mathcal{O}, \mathcal{R})$ consists of a node set $\mathcal{V}$, an edge set $\mathcal{E}$, a node type set $\mathcal{O}$, and a set $\mathcal{R}$ that consists of different edge types. We model each vehicle as a node in the graph, and each link between two vehicles as an edge. The nodes can be divide into three categories, $\mathcal{O} = \{O_1, O_2, O_3\}$, which correspond to the three types of vehicles. Meanwhile, we consider three types of edges $\mathcal{R} = \{R_{SC}, R_{SS}, R_I\}$, where R_{SC} represents the communication link between service provider vehicle and communication target vehicle, R_{SS} represents the sensing link between service provider vehicle and sensing target vehicle, and R_I represents the interference link between two service provider vehicles. Specifically, the feature of each vehicle is $\boldsymbol{f}_v = [e_{v1}, \ldots, e_{vM'}], \mathcal{V} \in \mathcal{K} \cup \mathcal{M} \cup \mathcal{N}, \mathcal{M}' = \mathcal{M} \cup \mathcal{N}$, where $\boldsymbol{f}_v \in \mathbb{R}^{L\times 1}$, and $L = (|\mathcal{M}| + |\mathcal{N}|)$ is the total number of target vehicles, and $e_{vm'}$ is the number of service provider vehicles within the line-of-sight link between vehicle v and vehicle m'. It evaluates the potential interference between the current vehicle and each target vehicle. The weight of the edge between vehicle v and vehicle v' is $g_{vv'} = \left(L_{vv'}^{\mathrm{A}} L_{vv'}^{\mathrm{F}}\right)^{-1}$ for all $v' \in \mathcal{V} \setminus \{v\}$ with $\boldsymbol{g}_{vv'} \in \mathbb{R}^{1\times 1}$.

B. Components of the GNN-based Algorithm

Next, we will introduce the components of the proposed GNN-based solution for problem (8). Then, we will explain its

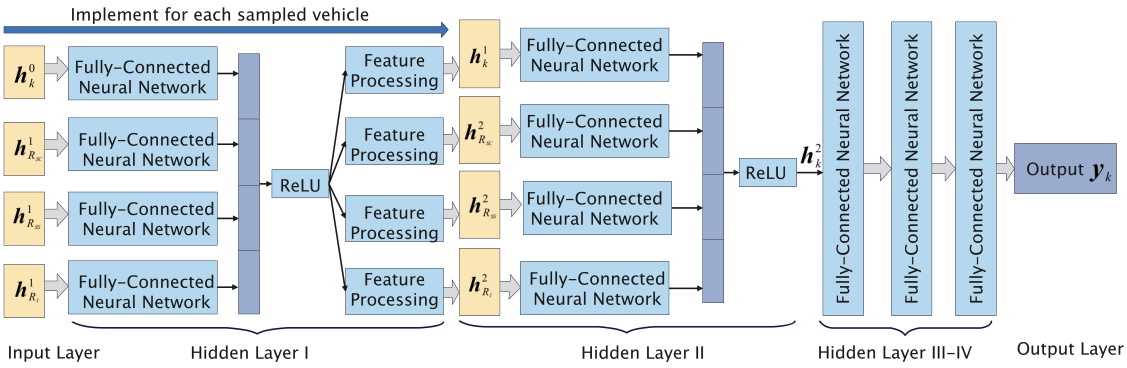

Fig. 2: Structure of the GNN model.

training process. The proposed GNN-based algorithm consists of four components: a) input layer, b) hidden layer I, c) hidden layer II, d) hidden layer III-V, and e) output layer, which are specified as follows:

- *Agent*: Our agent is a central controller that can obtain the geographic location of all vehicles. In each time slot, the central controller implements the designed GNN based algorithm to determine the service mode and user association for each service provider vehicle. Therefore, the controller actually executes the neural network $|\mathcal{K}|$ times so as to determine the service mode and user association for $|\mathcal{K}|$ vehicles.
- *Input Layer*: To determine the service mode of vehicle k and its serviced vehicles, the input of the designed scheme is based on the features of the vehicles that can connect to vehicle k. However, since the number of vehicles that can connect to different service provider vehicles are different, the size of input matrix may be different. To enable a neural network to extract graph information for different service provider vehicles that may connect to different number of service target vehicles, we use uniform sampling to calculate the average feature of each connected vehicle so as to fix the size of the input. In particular, we assume that the number of vehicles that the proposed algorithm needs to sample for a vehicle k is s_i in sampling iteration $i \in \{1, \cdots, I\}$. Meanwhile, we assume that the set of sampled vehicles that can directly connect to vehicle k as the set of first hop vehicles, which is represented by $\mathcal{L}^1(k)$ with $|\mathcal{L}^1(k)| = s_1$ being the number of vehicles in set $\mathcal{L}^1(k)$. The set of sampled vehicles that can connect to vehicle k via the first hop vehicles as the set of second hop vehicles and it is represented by $\mathcal{L}^2(k)$, where $\mathcal{L}^2(k) = \{\mathcal{L}^1(v') | v' \in \mathcal{L}^1(k)\}$. The number of vehicles in set $\mathcal{L}^2(k)$ is s_2. For example, in Fig. 3, the total number of sampled vehicles is 5 (set $s_1 = 2$ and $s_2 = 3$), $\mathcal{L}^1(k) = \{v_1, v_2\}$, and $\mathcal{L}^2(k) = \{v_3, v_4, v_5\}$. We assume that the subset of first hop vehicles with the type R edge is $\mathcal{L}^1_R(k)$. For example, in Fig. 3, $\mathcal{L}^1_{R_I}(k) = \{v_1\}$ and $\mathcal{L}^1_{R_{SS}}(k) = \{v_2\}$. Given these definitions, we next introduce the input of the proposed GNN-based method. From Fig. 2, we see that the input is connected to four fully connected layers and each fully connected layer has different inputs. The inputs to the four fully connected layers are: a) $\boldsymbol{h}^0_k = \boldsymbol{f}_k \in \mathbb{R}^{L\times 1}$, b) $\boldsymbol{h}^1_{R_{SC}} \in \mathbb{R}^{(L+1)\times 1}$, c) $\boldsymbol{h}^1_{R_{SS}} \in \mathbb{R}^{(L+1)\times 1}$, and d) $\boldsymbol{h}^1_{R_I} \in \mathbb{R}^{(L+1)\times 1}$, where

$$\boldsymbol{h}^1_{R_{SC}} = \frac{1}{|\mathcal{L}^1_{R_{SC}}(k)|} \sum_{v' \in \mathcal{L}^1_{R_{SC}}(k)} \boldsymbol{h}^0_{kv'}, \tag{9}$$

$$\boldsymbol{h}^1_{R_{SS}} = \frac{1}{|\mathcal{L}^1_{R_{SS}}(k)|} \sum_{v' \in \mathcal{L}^1_{R_{SS}}(k)} \boldsymbol{h}^0_{kv'}, \tag{10}$$

$$\boldsymbol{h}^1_{R_I} = \frac{1}{|\mathcal{L}^1_{R_I}(k)|} \sum_{v' \in \mathcal{L}^1_{R_I}(k)} \boldsymbol{h}^0_{kv'}, \tag{11}$$

with $\boldsymbol{h}^0_{kv'} = \left[\boldsymbol{h}^0_{v'} \| g_{kv'}\right]$, $\boldsymbol{h}^0_{kv'} \in \mathbb{R}^{(L+1)\times 1}$, $\cdot\|\cdot$ being the vector concatenation, $|\mathcal{L}^1_{R_{SC}}(k)|$, $|\mathcal{L}^1_{R_{SS}}(k)|$, and $|\mathcal{L}^1_{R_I}(k)|$ being the number of vehicles in set $\mathcal{L}^1_{R_{SC}}(k)$, $\mathcal{L}^1_{R_{SS}}(k)$, and $\mathcal{L}^1_{R_I}(k)$, respectively.

- *Hidden Layer I*: This layer consists of four fully-connected layers and it is used to extract the graph information of first hop vehicles of each vehicle k. The output of this layer is

$$\boldsymbol{h}^1_k = \sigma\left(\left[\boldsymbol{w}_1\boldsymbol{h}^0_k \| \boldsymbol{w}_2\boldsymbol{h}^1_{R_{SC}} \| \boldsymbol{w}_3\boldsymbol{h}^1_{R_{SS}} \| \boldsymbol{w}_4\boldsymbol{h}^1_{R_I}\right]\right), \tag{12}$$

where $\sigma(\cdot)$ is the rectified linear unit function (ReLU), $\boldsymbol{w}_1 \in \mathbb{R}^{(\lambda_0/4)\times L}$, $\boldsymbol{w}_2 \in \mathbb{R}^{(\lambda_0/4)\times(L+1)}$, $\boldsymbol{w}_3 \in \mathbb{R}^{(\lambda_0/4)\times(L+1)}$ and $\boldsymbol{w}_4 \in \mathbb{R}^{(\lambda_0/4)\times(L+1)}$ are the weight parameters of the four fully connected layers. λ_0 is the dimension of graph information vector, $\boldsymbol{w}_1$ is the weight matrix for the current vehicle, and $\boldsymbol{w}_2$, $\boldsymbol{w}_3$ and $\boldsymbol{w}_4$ are the weight matrices for the vehicles with the type R_{SC}, R_{SS}, and R_I edge, respectively. To support heterogeneity of nodes and edges, we set separate neighbourhood weight matrices $\boldsymbol{w}_2$, $\boldsymbol{w}_3$ and $\boldsymbol{w}_4$ for each type of vehicles. From (9) to (12), we extract only the graph information of vehicle v. However, we need the graph information of all sampled first hop vehicles to optimize mode selection and vehicle connection. Therefore, we need to execute (9) to (12) for each sampled vehicle (i.e., for s_1 times). After that, we can obtain $\boldsymbol{h}^1_{v'} \in \mathbb{R}^{\lambda_0\times 1}$, $\forall v' \in \mathcal{L}^1(k)$ for each sampled vehicle v'.

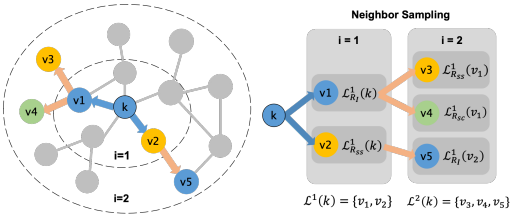

Fig. 3: An example of vehicle sampling.

- *Hidden Layer II*: This layer consists of four fully-connected layers and it is used to extract the graph information of second hop vehicles of vehicle k. From Fig. 2, we can see that the input to each fully connected layer in hidden layer II is different. The inputs to the four fully connected layers are: a) $\boldsymbol{h}_k^1 \in \mathbb{R}^{\lambda_0 \times 1}$, b) $\boldsymbol{h}_{R_{SC}}^2 \in \mathbb{R}^{(\lambda_0+1)\times 1}$, c) $\boldsymbol{h}_{R_{SS}}^2 \in \mathbb{R}^{(\lambda_0+1)\times 1}$, and d) $\boldsymbol{h}_{R_I}^2 \in \mathbb{R}^{(\lambda_0+1)\times 1}$, where

$$\boldsymbol{h}_{R_{SC}}^2 = \frac{1}{|\mathcal{L}_{R_{SC}}^1(k)|} \sum_{v' \in \mathcal{L}_{R_{SC}}^1(k)} \boldsymbol{h}_{kv'}^1, \tag{13}$$

$$\boldsymbol{h}_{R_{SS}}^2 = \frac{1}{|\mathcal{L}_{R_{SS}}^1(k)|} \sum_{v' \in \mathcal{L}_{R_{SS}}^1(k)} \boldsymbol{h}_{kv'}^1, \tag{14}$$

$$\boldsymbol{h}_{R_I}^2 = \frac{1}{|\mathcal{L}_{R_I}^1(k)|} \sum_{v' \in \mathcal{L}_{R_I}^1(k)} \boldsymbol{h}_{kv'}^1, \tag{15}$$

with $\boldsymbol{h}_{kv'}^1 = \left[\boldsymbol{h}_{v'}^1 \| g_{kv'}\right]$ and $\boldsymbol{h}_{kv'}^1 \in \mathbb{R}^{(\lambda_0+1)\times 1}$. The output of this layer is

$$\boldsymbol{h}_k^2 = \sigma\left(\left[\boldsymbol{w}_5 \boldsymbol{h}_k^1 \| \boldsymbol{w}_6 \boldsymbol{h}_{R_{SC}}^2 \| \boldsymbol{w}_7 \boldsymbol{h}_{R_{SS}}^2 \| \boldsymbol{w}_8 \boldsymbol{h}_{R_I}^2\right]\right), \tag{16}$$

where $\boldsymbol{h}_k^2 \in \mathbb{R}^{\lambda_0 \times 1}$, $\boldsymbol{w}_5 \in \mathbb{R}^{(\lambda_0/4)\times \lambda_0}$, $\boldsymbol{w}_6 \in \mathbb{R}^{(\lambda_0/4)\times(\lambda_0+1)}$, $\boldsymbol{w}_7 \in \mathbb{R}^{(\lambda_0/4)\times(\lambda_0+1)}$, and $\boldsymbol{w}_8 \in \mathbb{R}^{(\lambda_0/4)\times(\lambda_0+1)}$ are the weight parameters of the four fully connected layers, respectively. $\boldsymbol{w}_5$ is weight matrix for vehicle k and the others are the weight matrices for three types of second hop vehicles, i.e., $\boldsymbol{w}_6$ is the weight matrix for the vehicles with a type R_{SC} edge, $\boldsymbol{w}_7$ is the weight matrix for the vehicles with a type R_{SS} edge, and $\boldsymbol{w}_8$ is the weight matrix for the vehicles with a type R_I edge. Compared to the aggregate function in [12] that considers only node features, we consider both node features and edge weights in both hidden layers I and II. Here, the output $\boldsymbol{h}_k^2$ can be considered as the graph information of vehicle k, since it includes the graph information of sampled first hop and second hop vehicles.
- *Hidden Layers III-V*: Three fully-connected layers are used to find the relationship between the graph information vector $\boldsymbol{h}_k^2$ and the probability distribution of vehicle k servicing each target vehicle in the corresponding operating mode.
- *Output*: The output of the network, $\boldsymbol{y}_k = \left[y_k^1, \cdots, y_k^{L+1}\right]$, is the probability distribution of vehicle k servicing $L+1$ target vehicles in the corresponding operating mode. Here, $L+1$ is the total number of classification classes, including the case that vehicle k is not connected to any target vehicles.

Algorithm 1 GNN-based Method for the Joint Mode Selection and User Association Problem

Input: Vehicle features $\{\boldsymbol{f}_v, \forall v \in \mathcal{V}\}$, edge weights $\{g_{vv'}, \forall v' \in \mathcal{V} \setminus \{v\}\}$, and sampling size s_1 and s_2.
Initialize: $\boldsymbol{w}$, $\boldsymbol{p}$, and $\boldsymbol{b}$ are initially generated randomly via a uniform distribution;
$\boldsymbol{h}_v^0 \leftarrow \boldsymbol{f}_v$, $\boldsymbol{h}_{vv'}^0 \leftarrow \left[\boldsymbol{h}_{v'}^0 \| g_{vv'}\right]$, $\forall v \in \mathcal{V}, \forall v' \in \mathcal{V} \setminus \{v\}$;
for $k = 1 \rightarrow K$ **do**
  Sample the sets $\mathcal{L}^1(k)$ and $\mathcal{L}^2(k)$ with sampling size s_1 and s_2;
  Extract the graph information $\boldsymbol{h}_k^1$ of vehicle k based on (9)-(12);
  for $v' \in \mathcal{L}^1(k)$ **do**
    Aggregate the neighboring graph information vectors of vehicle v', $\boldsymbol{h}_{R_{SC}}^1$, $\boldsymbol{h}_{R_{SS}}^1$, and $\boldsymbol{h}_{R_I}^1$, based on (9)-(11);
    Concatenate the vehicle's current representation, $\boldsymbol{h}_{v'}^0$, with the aggregated neighborhood vector based on (12);
    Obtain the graph information $\boldsymbol{h}_{v'}^1$ of vehicle v';
  end for
  $\boldsymbol{h}_{kv'}^1 \leftarrow \left[\boldsymbol{h}_{v'}^1 \| g_{kv'}\right]$, $\forall v' \in \mathcal{L}^1(k)$;
  Aggregate the neighboring feature vectors of vehicle k, $\boldsymbol{h}_{R_{SC}}^2$, $\boldsymbol{h}_{R_{SS}}^2$, and $\boldsymbol{h}_{R_I}^2$, based on (13)-(15);
  Concatenate the vehicle's current representation, $\boldsymbol{h}_k^1$, with the aggregated neighborhood vector based on (16);
  Obtain the graph information vector $\boldsymbol{h}_k^2$ for vehicle k;
  Use $\boldsymbol{h}_k^2$ to predict the probability distribution $\boldsymbol{y}_k$ of vehicle k;
end for
Obtain the probability distribution $\boldsymbol{y}_k$ for each vehicle $k \in \mathcal{K}$;
Determine the mode selection and user association strategy by selecting $k_1^* = \arg\max_{k \in \mathcal{K}} \; y_k^m$ for all $m \in \mathcal{M}$, and $k_2^* = \arg\max_{k \in \mathcal{K}} \; y_k^{|\mathcal{M}|+n}$ for all $n \in \mathcal{N}$. Then, set $\alpha_{k_1^* m} = 1$ and $\beta_{k_2^* n} = 1$;
Reassign the vehicle k to sensing target vehicle n if the sensing service requirement is unsatisfied.
Output: The mode selection and user association indicator matrices, $\boldsymbol{\alpha}$ and $\boldsymbol{\beta}$.

C. Training of the Proposed GNN-based Algorithm

Given the components defined in the previous section, next, we introduce the entire procedure of training the proposed GNN based method. We use binary cross entropy (BCE) as the loss function to minimize the difference between the the predicted multi-label classification result and the actual multi-label classification result, which is given by

$$J(\boldsymbol{w}, \boldsymbol{p}, \boldsymbol{b}) = \sum_{l=1}^{L+1} -z_k^l \log \delta\left(y_k^l\right) - \left(1 - z_k^l\right) \log\left(1 - \delta\left(y_k^l\right)\right), \tag{17}$$

where $\delta(\cdot)$ is the sigmoid function, z_k^l is the label of vehicle k for class l, $\boldsymbol{w}$ is the weight matrix of hidden layer I, and $\boldsymbol{p}$ and $\boldsymbol{b}$ are the weight matrix and bias of hidden layer III-V, respectively. To minimize (17), we optimize $\boldsymbol{w}$, $\boldsymbol{p}$, and $\boldsymbol{b}$ using the back-propagation algorithm with the stochastic gradient descent (SGD) approach. The entire training process of the proposed algorithm is summarized in **Algorithm 1**.

IV. Simulation Results and Analysis

In our simulations, we consider a specific region of 100 m × 100 m. The detailed parameters are the same as Table II in [10]. The size of hidden layer III-V is set as $\{32, 64, 64\}$, the number of training iterations is 5,000, and σ is 1. The GPS dataset used to generate vehicle topologies is obtained from Shanghai Traffic Department [13]. For comparison purposes, we consider three baselines: baseline a) is an exhaustive search

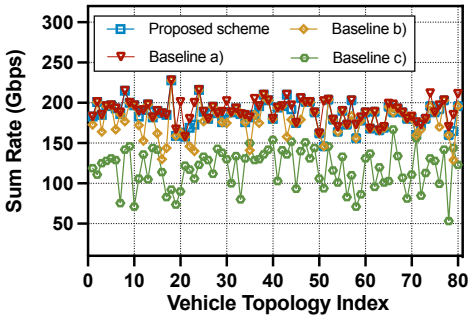

Fig. 4: The sum rate as the vehicle topology varies ($\lambda_0 = 64$, $s_1 = s_2 = 10$, $|\mathcal{K}| = 5$, $|\mathcal{M}| = 2$, and $|\mathcal{N}| = 2$).

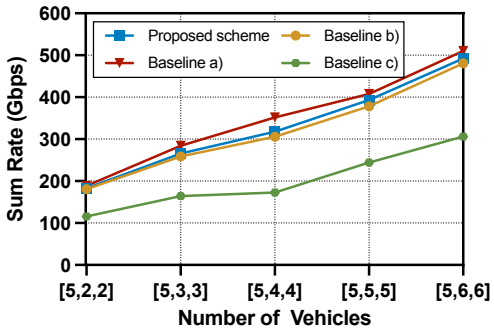

Fig. 5: The sum rate as the number of target vehicles varies ($\lambda_0 = 64$, $|\mathcal{K}| = 5$, $|\mathcal{M}|$ and $|\mathcal{N}|$ vary from 2 to 6).

algorithm, which can be considered as the optimal solution for problem (8), baseline b) is based on homogeneous graph. For comparison fairness, baseline b) uses the same neural network architecture as the proposed method, but a graph information extraction method from [14]. Baseline c) directly uses the geographic location information to optimize mode selection and user association scheme, without using GNNs to extract the graph information vectors.

Fig. 4 shows how the sum of data rates of all communication target vehicles change as the vehicle topology varies. In this figure, the location of service provider vehicles varies in different vehicle topologies while the location of service target vehicles is fixed. From Fig. 4, we see that the proposed scheme improves the sum rate by up to 3.95% and 36.16% compared to baselines b) and c). This is because the proposed scheme jointly considers the geographical location information and topological information and, hence, it can optimize user association and resource allocation to reduce the interlink interference. In Fig. 4, we can also observe that, there is only a slight performance gap between the proposed scheme and baseline a). This is because the proposed scheme enables the trained GNN to quickly adapt to changing vehicle topologies.

Fig. 5 shows how the sum of data rates of all communication target vehicles change as the number of communication and sensing target vehicles varies. From this figure, we can see that, as the number of communication and sensing target vehicles increase, the sum of data rates of all communication target vehicles increases since more communication links are established. Fig.5 also shows that, compared to baselines b) and c), the proposed scheme can achieve up to 2.78% and 34.85% gains in terms of sum rate. The is due to the fact that the proposed scheme considers the vehicle type impact on mode selection and user association. Fig.5 also shows that the gap between the proposed scheme and baseline a) is less than 6%. This indicates that the proposed GNN-based scheme can effectively decide the mode selection and user association strategy for service provider vehicles.

V. Conclusion

In this paper, we have developed a novel framework that uses THz for joint communication and sensing in vehicular networks. Our goal is to maximize the sum of data rates of all communication target vehicles while satisfying the sensing service requirements of all sensing target vehicles. To this end, we formulated an optimization problem that jointly considers service mode selection, user association, THz channel particularities, and fast-changing vehicle topologies. To solve this problem, we developed a novel heterogeneous GNN-based scheme. The proposed scheme enables the trained GNN to quickly adapt to the fast-changing vehicle topologies with various vehicle types. Simulation results verified that the proposed method can achieve significant gains.

References

[1] M. H. C. Garcia, A. Molina-Galan, M. Boban, J. Gozalvez, B. Coll-Perales, T. Sahin, and A. Kousaridas, "A tutorial on 5G NR V2X communications," *IEEE Communications Surveys & Tutorials*, vol. 23, no. 3, pp. 1972–2026, Thirdquarter 2021.

[2] C. Chaccour, M. N. Soorki, W. Saad, M. Bennis, P. Popovski, and M. Debbah, "Seven defining features of terahertz (THz) wireless systems: A fellowship of communication and sensing," *IEEE Communications Surveys & Tutorials*, vol. 24, no. 2, pp. 967–993, Secondquarter 2022.

[3] J. A. Zhang, M. L. Rahman, K. Wu, X. Huang, Y. J. Guo, S. Chen, and J. Yuan, "Enabling joint communication and radar sensing in mobile networks—A survey," *IEEE Communications Surveys & Tutorials*, vol. 24, no. 1, pp. 306–345, Firstquarter 2022.

[4] X. Mu, Y. Liu, L. Guo, J. Lin, and L. Hanzo, "NOMA-aided joint radar and multicast-unicast communication systems," *IEEE Journal on Selected Areas in Communications*, vol. 40, no. 6, pp. 1978–1992, June 2022.

[5] F. Liu, C. Masouros, A. Petropulu, H. Griffiths, and L. Hanzo, "Joint radar and communication design: Applications, state-of-the-art, and the road ahead," *IEEE Transactions on Communications*, vol. 68, no. 6, pp. 3834–3862, June 2020.

[6] Q. Zhang, X. Wang, Z. Li, and Z. Wei, "Design and performance evaluation of joint sensing and communication integrated system for 5G mmWave enabled CAVs," *IEEE Journal of Selected Topics in Signal Processing*, vol. 15, no. 6, pp. 1500–1514, Nov. 2021.

[7] B. Chang, X. Yan, L. Zhang, Z. Chen, L. Li, and M. A. Imran, "Joint communication and control for mmWave/THz beam alignment in V2X networks," *IEEE Internet of Things Journal*, vol. 9, no. 13, pp. 11 203–11 213, July 2022.

[8] Y. Wu, J. Kokkoniemi, C. Han, and M. Juntti, "Interference and coverage analysis for terahertz networks with indoor blockage effects and line-of-sight access point association," *IEEE Transactions on Wireless Communications*, vol. 20, no. 3, pp. 1472–1486, June 2021.

[9] M. T. Hossan and H. Tabassum, "Mobility-aware performance in hybrid RF and terahertz wireless networks," *IEEE Transactions on Communications*, vol. 70, no. 2, pp. 1376–1390, Feb 2022.

[10] A. Shafie, N. Yang, S. Durrani, X. Zhou, C. Han, and M. Juntti, "Coverage analysis for 3D terahertz communication systems," *IEEE Journal on Selected Areas in Communications*, vol. 39, no. 6, pp. 1817–1832, June 2021.

[11] M. Chen, U. Challita, W. Saad, C. Yin, and M. Debbah, "Artificial neural networks-based machine learning for wireless networks: A tutorial," *IEEE Communications Surveys & Tutorials*, vol. 21, no. 4, pp. 3039–3071, Fourthquarter 2019.

[12] CSIRO, "Stellargraph machine learning library," https://github.com/stellargraph/stellargraph, 2018.

[13] D. Zhao, Y. Gao, Z. Zhang, Y. Zhang, and T. Luo, "Prediction of vehicle motion based on markov model," in *Proc. International Conference on Computer Systems, Electronics and Control (ICCSEC)*, Dalian, China, Dec. 2017, pp. 205–209.

[14] Z. He, L. Wang, H. Ye, G. Y. Li, and B.-H. F. Juang, "Resource allocation based on graph neural networks in vehicular communications," in *Proc. IEEE Global Communications Conference*, Taipei, Taiwan, Dec. 2020, pp. 1–5.